104 (2025) 105392

Contents lists available at ScienceDirect

Poultry Science

journal homepage: www.elsevier.com/locate/psj

Selenomethionine alleviates LPS-induced PANoptosis in chicken cecum through the ROS/MAPK pathway, thereby mitigating inflammation and microbial dysbiosis

Dan Chen [a,1], Huanyi Liu [a,1], Wenying Sun [a], Shiwen Xu [a,b,c,*]

[a] College of Veterinary Medicine, Northeast Agricultural University, Harbin 150030, China
[b] Key Laboratory of the Provincial Education Department of Heilongjiang for Common Animal Disease Prevention and Treatment, College of Veterinary Medicine, Northeast Agricultural University, Harbin, 150030, China
[c] Laboratory of Embryo Biotechnology, College of Life Science, Northeast Agricultural University, Harbin, 150030, China

ARTICLE INFO

Keywords:
SeMet
ROS/MAPK
PANoptosis
inflammatory
Intestinal flora

ABSTRACT

Selenomethionine (SeMet), a vital organic selenium compound, plays a pivotal role in maintaining redox homeostasis and is extensively utilized as a dietary supplement. The ROS/MAPK signaling axis has been implicated in mediating the detrimental effects of exogenous toxins on biological systems. However, the potential involvement of the ROS/MAPK signaling pathway in the protective mechanism of organic selenium against LPS-induced cecal injury in chickens remains to be elucidated. In this study, 80 Hailan brown laying hens aged 46 weeks were randomly allocated into four experimental groups ($n = 20$) to establish a model for evaluating the effects of dietary SeMet supplementation and/or LPS treatment. The experimental design comprised the following groups: the C group (basal diet), the SeMet -supplemented group (SeMet group), the LPS-treatment group (LPS group), and the combined SeMet and LPS treatment group (Se+LPS group). Results showed that SeMet mitigated LPS-induced cecal epithelial disruption, oxidative stress (ROS, H_2O_2, and MDA), and restored antioxidant enzyme activity. SeMet also suppressed MAPK signaling and PANoptosis-related protein expression (GSDMD, Caspase-3, MLKL), while enhancing intestinal tight junctions and reducing inflammation. Additionally, SeMet restored gut microbiota homeostasis. These findings demonstrate that SeMet alleviates LPS-triggered cecal PANoptosis by inhibiting the ROS/MAPK cascade, improving intestinal barrier function, and modulating microbial balance. Our findings provide novel insights into dietary SeMet as a potential nutritional strategy to mitigate cecal injury in poultry, with implications for improving gut health and productivity in commercial laying hens.

Introduction

An indispensable trace element for maintaining health in both humans and animals, selenium (Se) carries out its fundamental biological activities primarily by incorporation into selenoproteins, thereby playing an essential part in developmental processes and defense against oxidative damage (Wang et al., 2021). Se acts as a powerful antioxidant by promoting intracellular reactive oxygen species (ROS) scavenging and protecting cellular membranes and DNA from oxidative injury through diverse enzymatic antioxidant mechanisms (Li et al., 2017). Clinical evidence connects inadequate Se consumption through diet with multiple pathological manifestations, notably Keshan disease, immunological disorders, and white muscle disease (Chen et al., 2024). Epidemiological studies have revealed that inadequate Se intake in adolescents correlates with elevated plasma oxidative products, contributing to obesity, developmental delays, and increased susceptibility to malignant diseases (Soares de Oliveira et al., 2021). Notably, dietary Se supplementation has been demonstrated to effectively correct redox imbalances and significantly mitigate oxidative stress (Li et al., 2025; Zhou et al., 2025). While inorganic Se has been widely utilized in animal husbandry due to its cost-effectiveness, its limitations, including low bioavailability and high toxicity, have led to its prohibition or restriction

All authors have read the manuscript and agreed to submit it in its current form for consideration for publication in the Journal.

* Corresponding author at: Northeast Agricultural University, Harbin 150030, China.
E-mail address: shiwenxu@neau.edu.cn (S. Xu).

[1] Dan Chen and Huanyi Liu contributed equally to this manuscript.

https://doi.org/10.1016/j.psj.2025.105392
Received 17 April 2025; Accepted 3 June 2025
Available online 4 June 2025

in countries such as Japan and Sweden (Mahima et al., 2012; Pecoraro et al., 2022). In recent years, SeMet, an organic Se source characterized by high bioavailability and low toxicity, has emerged as a focal point in Se nutrition research (Kong et al., 2025; Xia et al., 2025). Research has demonstrated that SeMet mediates its antioxidative properties by regulating the KEAP1/Nrf2/HO-1 signaling axis, significantly mitigating LPS-induced inflammatory responses and necrotic damage in the eggshell gland (Chen et al., 2024). Current studies verify that dietary SeMet administration shields rabbits from AFB1-induced oxidative liver damage while preserving normal gut microbiota composition (Kong et al., 2025). Furthermore, studies have revealed that SeMet reduces LPS-triggered apoptotic cell death and inflammatory responses in avian cardiomyocytes through dual mechanisms of oxidative stress suppression and JAK2/STAT3/A20 pathway inhibition (Lei et al., 2024).

The mitogen-activated protein kinase (MAPK) family represents a crucial signaling cascade comprising three distinct members: extracellular signal-regulated kinase (ERK), p38, and c-Jun N-terminal kinase (JNK) (Lee et al., 2020). Positioned at a pivotal junction of cellular signaling pathways, MAPKs serve as central regulators of cellular stress responses, inflammation, necroptosis, and apoptosis (Wang et al., 2025). Investigations in swine testicular cells have revealed that microplastic exposure activates the JNK/ERK/p38 pathway through ROS generation, subsequently elevating Caspase-3 and RIPK1 levels to induce both apoptosis and necroptosis (Wang et al., 2022). Analogous mechanisms occur in high-fat diet-associated kidney injury, where ROS-mediated JNK/ERK/p38 pathway activation promotes programmed cell death and enhances production of pro-inflammatory signaling molecules (Jia et al., 2025). Studies reveal that chemical activation of the ERK pathway results in NLRP3 inflammasome formation, which subsequently drives apoptosis and IL-1β production (Song et al., 2025). Recent studies have have defined PANoptosis as a unique form of regulated cell death marked by the co-activation of three distinct death pathways: apoptosis, pyroptosis, and necroptosis (Song et al., 2025). This complex, inflammatory-regulated cell death process is initiated by specific triggers and modulated by the PANoptosome complex (Pandeya and Kanneganti, 2024). Emerging evidence demonstrates that ischemia/reperfusion injury induces microglial release of miRNA-423-5P, subsequently activating the MAPK pathway and triggering neuronal PANoptosis (Lan et al., 2024). Zhou et al. have further elucidated that bacterial infections exacerbate sepsis-associated PANoptosis through activation of the JNK/ERK/p38 signaling pathway (Zhou et al., 2022). Additionally, various viral infections have been shown to induce PANoptosis by promoting phosphorylation of JNK/ERK/p38, thereby regulating cell death and inflammatory responses (Udawatte and Rothman, 2021). Growing research findings highlight the pivotal involvement of PANoptosis in the development and progression of various pathological conditions. For instance, PANoptosis-mediated inflammatory responses are closely associated with myocardial injury and ventricular remodeling. In murine models, burn injuries have been shown to induce PANoptosome complex formation, leading to renal dysfunction and the development of nephritis (Yang et al., 2025).

As a key anatomical structure within the large intestine, the cecum represents the most significant fermentation organ in omnivores and herbivores, contributing to nutrient absorption, immune system function, and maintenance of bacterial balance (Ballout et al., 2025). Existing scientific evidence demonstrates SeMet's capacity to counteract inflammatory processes in multiple organ systems across avian and mammalian species. Nevertheless, the molecular mechanisms by which SeMet mitigates LPS-induced cecal damage in poultry remain poorly understood. Therefore, the chicken model treated with SeMet or/and LPS was established in this study. Morphological observation was used to evaluate the injury of cecum. TUNEL staining, DHE staining, immunofluorescence staining, 16S rDNA sequencing, Western blotting and qRT PCR were used to evaluate ROS/MAPK pathway, oxidative stress PANoptosis, changes of inflammatory cytokines, tight junction proteins and intestinal flora. The present research aims to uncover the fundamental mechanisms by which SeMet alleviates LPS-triggered gut damage, providing practical insights for dietary Se supplementation in poultry production systems.

Materials and methods

Animals and experimental design

All procedures used in the study were approved by the institutional animal care and use Committee of Northeast Agricultural University (SRM11). A total of 80 healthy 46-week-old Hyland brown laying hens were randomly allocated into four experimental groups, including group C, LPS group, Se group and LPS+Se group. The chickens in group C and LPS were fed a basal diet without additional SeMet. Dietary supplementation with 0.75 mg/kg Se in the form of SeMet was provided to both the Se group and SeMet + LPS group. The detailed composition of the experimental diets is presented in Table S1. Except for dietary Se levels, all husbandry parameters including ambient temperature, relative humidity, and photoperiod were kept identical between experimental groups. The chickens had unrestricted availability of food and water throughout the study. After 6 weeks of feeding, experimental groups LPS and LPS+Se were injected intravenously with 0.2 mg/kg LPS to create an acute inflammation model. Intravenous administration of isovolumetric 0.9 % sterile saline was performed in both C and Se groups. After 12 h, animals were euthanized and cecal tissues were immediately processed for preservation in 10 % formalin, 2.5 % glutaraldehyde, or liquid nitrogen storage. The dose selection of SeMet and LPS is based on previous research results. 0.75mg/kg Se can significantly improve the antioxidant capacity of poultry without toxic effect, while 0.2mg/kg LPS has been proved to be able to effectively induce chicken inflammatory reaction and ensure the survival rate of experimental animals (Chen et al., 2024; Zhang et al., 2021; Tang et al., 2021).

Hematoxylin and Eosin (H&E) Staining

Following established protocols (Yang et al., 2025), fixed cecal samples underwent sequential alcohol dehydration, paraffin embedding, and microtome sectioning at 5 μm thickness. Tissue sections were then processed through xylene deparaffinization and alcohol rehydration before H&E staining. Final histological assessment was conducted via light microscopic observation and photomicrography. Cecal lesions were systematically scored using a validated histopathological scale evaluating seven distinct criteria: inflammatory cell accumulation, tissue injury magnitude, proliferative response, goblet cell disappearance, ulcerative areas, fibrovascular tissue proliferation, and glandular density reduction, following published methodology (Burrello et al., 2018).

Transmission electron microscopy (TEM)

Glutaraldehyde-fixed cecal tissues (2.5 %, 24 h) were phosphate-buffer washed before osmium tetroxide post-fixation (1 %). Ethanol-acetone dehydration preceded epoxy resin embedding. Ultrathin sections were contrast-enhanced with uranyl-lead stains and imaged on a Hitachi H7650 TEM (Osaka, Japan). Quantitative assessment of microvilli, enterocytes, and zonula occludens damage employed validated ultrastructural criteria (Zhang et al., 2019).

Quantitative real-time PCR (qRT-PCR)

Cecal tissue RNA isolation was performed with TRIzol reagent, followed by cDNA synthesis employing the KR106 FastQuant RT Kit (Tiangen Biotech, China). Quantitative PCR analysis was conducted on a CFX96 system using 20 μL reactions containing 0.3 μM primers, prepared with FP205 SuperReal PreMix Plus (SYBR Green, Tiangen

Biotech) (Lu et al., 2024). β-actin was used as the internal reference gene for normalization, and relative mRNA expression levels were calculated using the $2^{-\Delta\Delta Ct}$ method. The primer sequences used in this study are summarized in Table S2.

Western blotting

Homogenized cecal samples in RIPA lysis buffer (Solarbio) were centrifuged to obtain protein lysates. Electrophoretically separated proteins were transferred to NC membranes, which were then blocked (5 % skim milk, 37°C, 2 h), incubated with primary antibodies (4°C, overnight), and exposed to secondary antibodies (room temperature, 2 h) (Wang et al., 2020). Protein signals were captured using a Bio-Rad imaging workstation and quantified with ImageJ software, using β-actin as internal reference. Complete antibody information appears in Table S3.

Oxidative stress level detection

Reactive oxygen species (ROS) were quantified via dihydroethidium (DHE, Beyotime S0063) fluorescence staining, with tissue sections incubated in DHE working solution (37°C, dark conditions, 30 min) per protocol. The intracellular levels of hydrogen peroxide (H_2O_2), total protein (TP), inducible nitric oxide synthase (iNOS), malondialdehyde (MDA), glutathione (GSH), superoxide dismutase (SOD), catalase (CAT), glutathione peroxidase (GPX), and total antioxidant capacity (T-AOC) in cecal tissues were measured using commercially available detection kits from the Nanjing Jiancheng Bioengineering Institute (Nanjing, China).

Immunofluorescence staining

Cecal tissue sections were subjected to deparaffinization and rehydration. Subsequent to epitope recovery, 5 % serum-based blocking solution (Vivacell) was applied for 30 min. After washing, primary antibody incubation was performed at 4°C for approximately 16 h. Following day, tissue sections received 1-hour secondary antibody incubation. After 4-hour fixation in 4 % PFA (4°C), triple TBS washes (5 min each) preceded 1-hour blocking with shaking. Primary antibodies targeting tight junction proteins (occludin/ZO-1, Abclonal, 1:200) were applied overnight (4°C). Post quintuple TBS washes, BioDragon IgG secondaries (1:1000) incubated for 2 hours. Nuclear counterstaining used DAPI (15 min, dark) before fluorescence microscopy imaging.

Terminal deoxynucleotidyl transferase dUTP nick-end labeling (TUNEL) assay

DNA fragmentation was assessed with the commercial TUNEL kit (C1086, Beyotime) per manufacturer's guidelines. Prior to staining, tissue sections were sequentially processed with proteinase K and hydrogen peroxide solutions. The sectioning and staining procedures followed our previously published protocols (Liu et al., 2023; Xu et al., 2024). Nuclei were counterstained with DAPI for visualization of cecal tissue.

Intestinal microbiota analysis

For microbial analysis, cecal contents were aseptically collected immediately after dissection. The cecum was exteriorized, longitudinally incised, and approximately 0.5-1.0 g of central luminal material was collected using sterile instruments while avoiding mucosal contact. Samples were promptly transferred to DNA-free cryovials and processed within 15 min. DNA extraction followed an optimized CTAB/SDS protocol, with quality verified by electrophoresis (1 % agarose gel) and spectrophotometry. For optimal DNA integrity preservation, specimens were immediately aliquoted into sterile cryovials, snap-frozen in liquid nitrogen, and maintained at −80°C during storage and transport to Zhongke New Life Biotechnology Co., Ltd. The 16S rDNA sequencing was performed on the Illumina MiSeq PE250/PE300 platform following rigorous quality control procedures. The V3-V4 hypervariable regions were amplified using barcoded primers (341F-806R) with Phusion® High-Fidelity PCR Master Mix under standardized thermal cycling conditions: initial denaturation at 98°C for 1 min, followed by 30 cycles of denaturation (98°C, 10 s), annealing (50°C, 30 s), and elongation (72°C, 60 s), with a final extension at 72°C for 5 min. PCR products were quantified, purified using the AxyPrep DNA Gel Extraction Kit, and library preparation was conducted with the NEB Next® Ultra™ DNA Library Prep Kit following manufacturer protocols. Bioinformatic processing included quality filtering, OTU clustering at 97 % similarity, and taxonomic classification against reference databases. Community structure was evaluated through alpha/beta diversity metrics and differential abundance analysis.

Statistical analysis

All experiments were performed in triplicate, and data were visualized using GraphPad Prism 9.0. Statistical analysis was conducted using IBM SPSS 26.0, with one-way analysis of variance (ANOVA) applied to assess differences among groups. The experimental results are represented by the mean ± SD in the bar chart, or by the median IQR in the box chart and violin chart. The complete mean and SD values can be obtained in the supplementary table S4-S8. Duncan's multiple range test was used for post-hoc comparisons, with significance levels denoted as $^{*}P < 0.05$, $^{**}P < 0.01$, $^{***}P < 0.001$, and $^{****}P < 0.0001$.

Result

SeMet significantly mitigates LPS-induced pathological damage in cecal

Histopathological examination showed normal cecal morphology in both C and SeMet groups, with tightly arranged villi, scarce inflammatory cells, slight epithelial hyperplasia, numerous goblet cells, and absence of ulcerative changes or glandular degeneration. In contrast, the LPS group displayed extensive inflammatory cell infiltration in cecal tissues, severe cellular proliferation, significant loss of goblet cells, ulceration, and glandular atrophy ($P < 0.001$). Notably, SeMet treatment markedly attenuated these LPS-induced pathological alterations ($P < 0.05$; Fig. 1A-B). TEM further demonstrated that the C group and SeMet group maintained smooth nuclear membranes, intact mitochondrial and endoplasmic reticulum structures, and normal microvilli, epithelial cells, and tight junctions. In the LPS group, nuclear membrane rupture, mitochondrial swelling, cristae disappearance, and damage to microvilli, epithelial cells, and tight junctions were observed ($P < 0.0001$). Importantly, SeMet supplementation effectively reversed these LPS-induced ultrastructural changes ($P < 0.001$), preserving nuclear integrity and maintaining mitochondria with clear structural features (Fig. 1C-D).

SeMet alleviates LPS induced oxidative stress in cecal

To investigate the impact of SeMet on oxidative stress levels, we initially performed DHE staining on cecal tissues. DHE is reduced to fluorescent compounds under conditions of cellular oxidative stress. Comparative measurements confirmed LPS-induced oxidative stress elevation in intestinal tissues compared to the C group, demonstrated by enhanced red fluorescence emission ($P < 0.0001$). However, the SeMet+LPS group exhibited markedly reduced fluorescence intensity ($P < 0.001$), indicating suppression of oxidative stress levels relative to the LPS group (Fig. 2A). Concurrently, LPS treatment inhibited the activation of the Keap1/Nrf2 antioxidant signaling pathway. At the transcriptional level, LPS treatment significantly downregulated mRNA expression of Nrf2 ($P < 0.01$), HO-1 ($P < 0.001$), and NQO1 ($P < 0.01$), while upregulating Keap1 mRNA expression ($P < 0.0001$) compared to

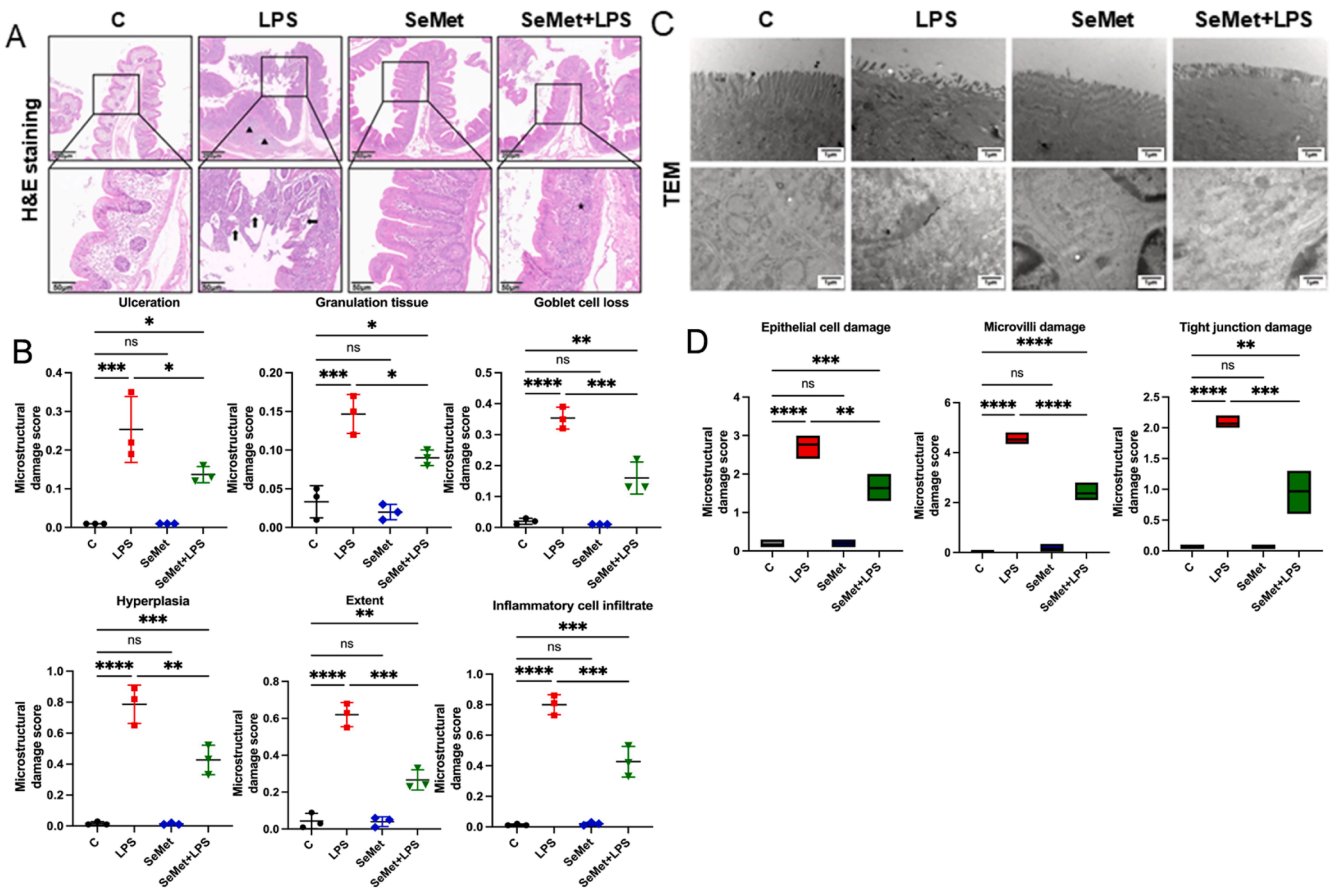

Fig. 1. Pathological observations of chicken cecal following treatment with SeMet and/or LPS. (A) H&E staining of chicken cecal tissue. Black triangles indicate inflammatory cell infiltration, and black arrows denote mucosal rupture. Scale bars: 200 μm and 50 μm. (B) Score of cecal microstructural damage, $n = 3$. (C) TEM images of chicken cecal tissue. Scale bar: 1 μm. (D) Score of cecal ultrastructure damage, $n = 3$.

the C group. SeMet supplementation effectively reversed these LPS-induced transcriptional alterations, restoring Nrf2 ($P < 0.05$), HO-1 ($P < 0.05$), and NQO1 ($P < 0.05$) mRNA levels, and normalizing Keap1 expression ($P < 0.001$; Fig. 2B-C). Consistent with the mRNA results, Western blot analysis revealed that LPS exposure substantially decreased protein levels of Nrf2 ($P < 0.0001$), HO-1 ($P < 0.001$), and NQO1 ($P < 0.0001$), but increased Keap1 protein expression ($P < 0.001$) relative to the C group. Importantly, SeMet co-treatment significantly ameliorated these protein expression changes, upregulating Nrf2 ($P < 0.01$), HO-1 ($P < 0.05$), and NQO1 ($P < 0.01$) while downregulating Keap1 ($P < 0.001$; Fig. 2D-E). The LPS-exposed group exhibited significant decreases in enzymatic antioxidants, including GPx ($P < 0.01$), SOD ($P < 0.01$), and CAT ($P < 0.0001$), along with reduced GSH concentration ($P < 0.01$). This was accompanied by increased expression of lipid peroxidation products, including iNOS ($P < 0.001$), H_2O_2 ($P < 0.0001$), and MDA ($P < 0.0001$), leading to impaired overall antioxidant potential in cecal tissues. Notably, SeMet co-administration with LPS substantially improved antioxidant capacity, as evidenced by restored GPX ($P < 0.05$), SOD ($P < 0.05$), and CAT ($P < 0.001$) activities, while effectively attenuating oxidative stress markers iNOS ($P < 0.01$), H_2O_2 ($P < 0.01$), and MDA ($P < 0.0001$; Fig. 2F).

SeMet inhibits LPS induced activation of MAPK signaling pathway

To elucidate MAPK pathway involvement in SeMet and/or LPS-mediated cecal responses, we quantitatively evaluated MAPK-associated markers using both qPCR and Western blot analyses. Experimental data demonstrated that neither the C group nor the SeMet group exhibited significant changes in MAPK pathway-related gene expression, including JNK ($P > 0.05$), ERK ($P > 0.05$), and p38 ($P > 0.05$). Similarly, no notable alterations were observed in the phosphorylation levels of their corresponding proteins: p-JNK ($P > 0.05$), p-ERK ($P > 0.05$), and p-p38 ($P > 0.05$). In contrast, LPS treatment robustly activated the MAPK signaling pathway. At the transcriptional level, LPS significantly upregulated the mRNA expression of JNK ($P < 0.0001$), ERK ($P < 0.0001$), and p38 ($P < 0.0001$). Concurrently, the phosphorylation levels of these kinases were markedly elevated, as evidenced by increased p-JNK ($P < 0.0001$), p-ERK ($P < 0.001$), and p-p38 ($P < 0.0001$). Notably, SeMet supplementation effectively counteracted LPS-induced MAPK pathway activation. Specifically, SeMet significantly attenuated the LPS-induced upregulation of JNK mRNA ($P < 0.0001$), ERK mRNA ($P < 0.0001$), and p38 mRNA ($P < 0.0001$). At the protein level, SeMet administration markedly reduced the phosphorylation of p-JNK ($P < 0.0001$), p-ERK ($P < 0.01$), and p-p38 ($P < 0.01$), indicating its potent inhibitory effect on MAPK signaling hyperactivation (Fig. 3A-D).

SeMet inhibits LPS-induced assembly of PANoptosomes in cecum

PANoptosomes, as dynamic multiprotein complexes, involve the assembly of ZBP1-mediated molecular scaffolds and the coordinated action of multiple cross-pathway proteins. Molecular analyses demonstrated that, compared to the C group, LPS stimulation significantly promoted PANoptosome assembly. At the mRNA level, LPS upregulated expression of the molecular scaffold ZBP1 ($P < 0.0001$), apoptosis-related components FADD ($P < 0.001$) and Caspase8 ($P < 0.0001$), necroptosis-related kinases RIPK1 ($P < 0.0001$) and RIPK3 ($P < 0.0001$), as well as pyroptosis-related components NLRP3 ($P < 0.001$), Caspase1

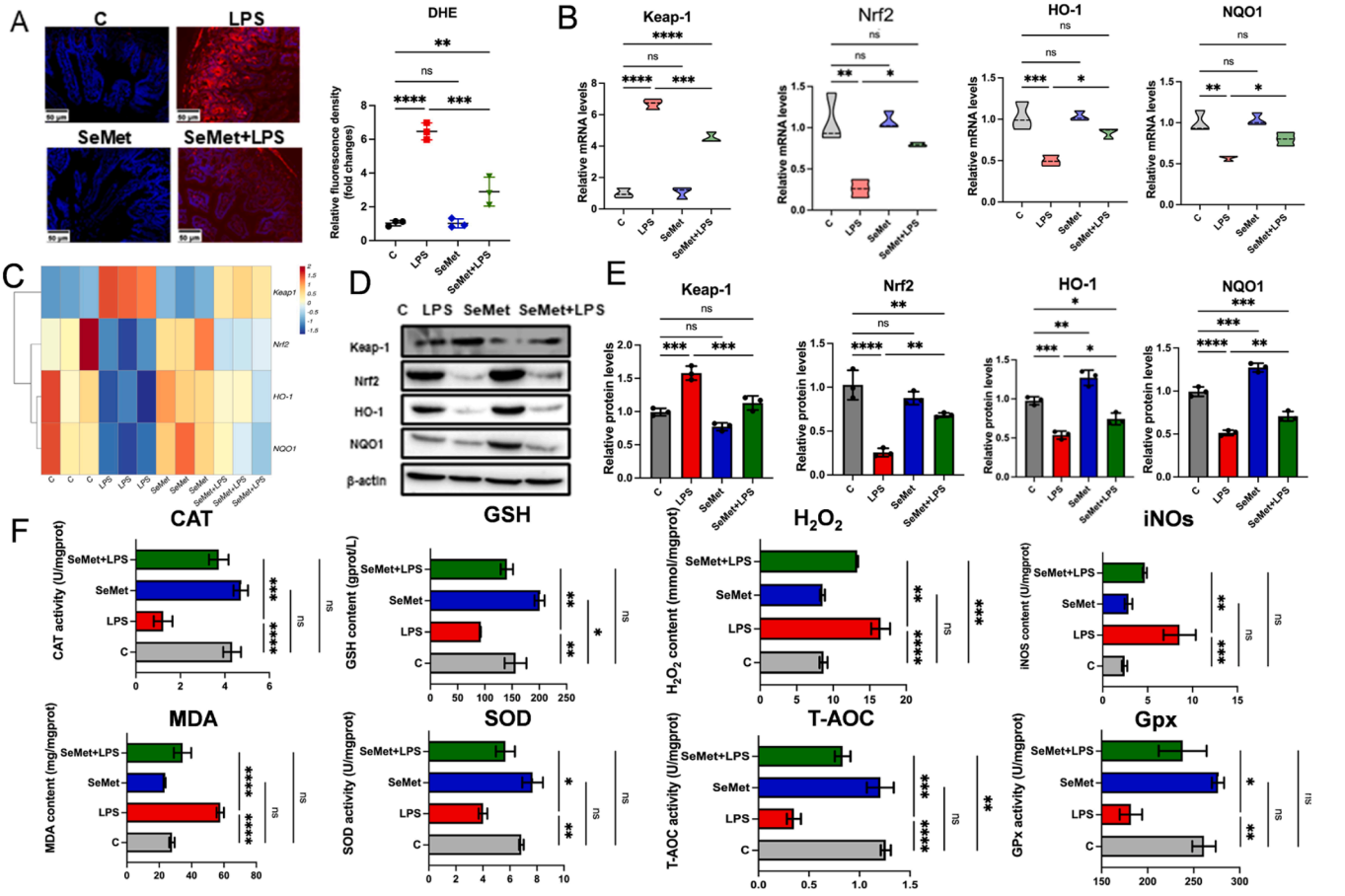

Fig. 2. Effects of SeMet and/or LPS on oxidative stress in the cecum of chickens. (A) DHE staining of chicken cecum. Scale bar: 50 μm. (B) qPCR results of Keap1/Nrf2/HO-1 pathway-related indicators, $n = 3$. (C) Heatmap depicting mRNA expression changes of Keap1/Nrf2/HO-1 pathway-related indicators, $n = 3$. (D Western blot analysis of Keap1/Nrf2/HO-1 pathway-related proteins, $n = 3$. (E) Quantitative results of protein expression changes in Keap1/Nrf2/HO-1 pathway-related indicators, $n = 3$. (F) Results of antioxidant enzyme activity and lipid peroxide levels, $n = 3$.

($P < 0.0001$) and ASC ($P < 0.001$). Corresponding increases were observed at protein levels for ZBP1 ($P < 0.0001$), FADD ($P < 0.0001$), Caspase8 ($P < 0.0001$), RIPK1 ($P < 0.0001$), RIPK3 ($P < 0.0001$), NLRP3 ($P < 0.0001$) and ASC ($P < 0.0001$). Notably, compared to LPS treatment alone, the combined SeMet+LPS intervention significantly suppressed PANoptosome assembly. At the mRNA level, SeMet downregulated expression of structural component ZBP1 ($P < 0.01$), apoptosis-related components FADD ($P < 0.001$) and Caspase8 ($P < 0.001$), necroptosis-related kinases RIPK1 ($P < 0.0001$) and RIPK3 ($P < 0.0001$), as well as pyroptosis-related components NLRP3 ($P < 0.01$), Caspase1 ($P < 0.05$) and ASC ($P < 0.001$). At the protein level, SeMet reduced expression of ZBP1 ($P < 0.001$), FADD ($P < 0.0001$), Caspase8 ($P < 0.05$), RIPK1 ($P < 0.05$), RIPK3 ($P < 0.001$), NLRP3 ($P < 0.0001$) and ASC ($P < 0.001$) (Fig. 4A-D).

SeMet attenuates LPS-induced cecal PANoptosis

PANoptosis represents a novel form of programmed cell death characterized by the simultaneous activation of apoptosis, necroptosis, and pyroptosis pathways. TUNEL staining of cecal tissues revealed that while the C group and SeMet group showed minimal green fluorescence, the LPS group exhibited significantly increased fluorescence intensity, indicating extensive DNA fragmentation characteristic of PANoptosis. SeMet supplementation markedly attenuated this effect (Fig. 5A). At the transcriptional level, LPS markedly upregulated expression of apoptosis executor Caspase3 ($P < 0.0001$), pyroptosis effector GSDMD ($P < 0.0001$), and necroptosis marker MLKL ($P < 0.0001$). These changes were accompanied by corresponding increases in protein levels for Caspase3 ($P < 0.001$), GSDMD-N ($P < 0.0001$), and MLKL ($P < 0.0001$). Importantly, SeMet treatment effectively attenuated these LPS-induced effects. At the mRNA level, SeMet significantly reduced expression of Caspase3 ($P < 0.0001$), GSDMD ($P < 0.01$), and MLKL ($P < 0.01$). Similarly, at the protein level, SeMet decreased expression of Caspase3 ($P < 0.01$), GSDMD-N ($P < 0.01$), and MLKL ($P < 0.001$). These findings collectively demonstrate that SeMet significantly mitigates LPS-induced PANoptosis through coordinated suppression of all three cell death pathways (Fig. 5B-E).

SeMet effectively mitigates LPS-induced cecal inflammation, tight junction disruption, andi flora disorder

To comprehensively evaluate the protective effects of SeMet on intestinal inflammation and epithelial barrier integrity, we conducted systematic analyses of inflammatory mediators and tight junction components. qPCR and Western blot results demonstrated LPS-induced increases in pro-inflammatory markers: TNF-α (mRNA $P < 0.0001$, protein $P < 0.001$), COX-2 (mRNA $P < 0.0001$, protein $P < 0.0001$), NF-κB (mRNA $P < 0.001$, protein $P < 0.01$), IL-6 (mRNA $P < 0.0001$, protein $P < 0.0001$), IL-1β (mRNA $P < 0.0001$, protein $P < 0.0001$), and PGE (mRNA $P < 0.0001$, protein $P < 0.0001$) compared to the C group. Concurrently, LPS suppressed the anti-inflammatory cytokine IL-4 (mRNA $P < 0.001$, protein $P < 0.001$). SeMet treatment effectively reversed these inflammatory changes, significantly reducing expression of TNF-α (mRNA $P < 0.0001$, protein $P < 0.001$), COX-2 (mRNA $P <$

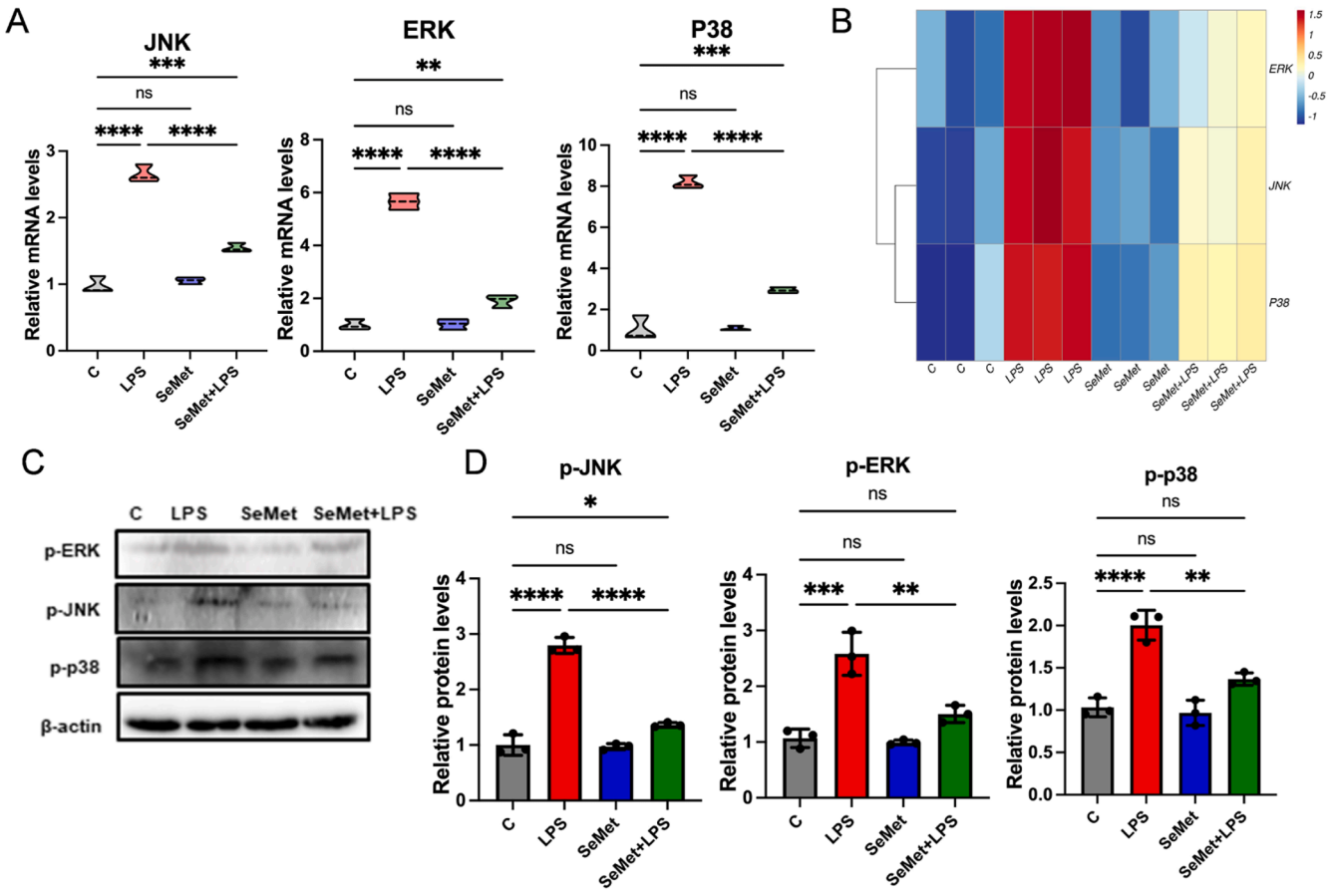

Fig. 3. Effects of SeMet and/or LPS on the MAPK signaling pathway in chicken cecal tissue. (A) qPCR results of MAPK pathway-related indicators, $n = 3$. (B) Heatmap illustrating mRNA expression changes of MAPK pathway-related indicators, $n = 3$. (C) Western blot analysis of MAPK pathway-related proteins, $n = 3$. (D) Quantitative results of protein expression changes in MAPK pathway-related indicators, $n = 3$.

0.0001, protein $P < 0.001$), NF-κB (mRNA $P < 0.05$, protein $P < 0.05$), IL-6 (mRNA $P < 0.001$, protein $P < 0.001$), IL-1β (mRNA $P < 0.0001$, protein $P < 0.0001$), and PGE (mRNA $P < 0.0001$, protein $P < 0.0001$) versus the LPS group. Additionally, SeMet restored IL-4 expression (mRNA $P < 0.01$, protein $P < 0.05$). Immunofluorescence revealed enhanced signals for occludin ($P < 0.001$) and ZO-1 ($P < 0.01$) in SeMet+LPS groups compared to LPS-treated samples. Molecular analyses confirmed SeMet-mediated restoration of tight junction components at both mRNA (ZO-1: $P < 0.05$; claudin-1: $P < 0.05$; occludin: $P < 0.05$) and protein levels (ZO-1: $P < 0.05$; claudin-1: $P < 0.05$; occludin: $P < 0.001$) relative to LPS treatment. These findings collectively demonstrate that SeMet administration maintains intestinal homeostasis by simultaneously modulating inflammatory responses and preserving epithelial barrier function (Fig. 6A-F).

Microbial composition changes associated with SeMet treatment were evaluated through comprehensive 16S rDNA sequencing of intestinal flora samples. Microbial analysis revealed that LPS administration disrupted intestinal microbiota homeostasis in chickens, marked by elevated abundance of pathogenic bacterial species. The Shannon index, a measure of α-diversity, was significantly reduced in the LPS-treated group compared to the C group ($P < 0.01$), indicating that LPS exposure disrupted the gut microbiota by decreasing both species richness and evenness. In contrast, co-administration of SeMet with LPS significantly restored the Shannon index to levels comparable to the control ($P < 0.05$ vs. LPS group), suggesting that Se effectively mitigated the LPS-induced dysbiosis (Fig. 7A). Principal coordinate analysis (PCA) based on Bray-Curtis distances demonstrated distinct clustering patterns among groups (Fig. 7B). The LPS group exhibited significant separation from the C group along the primary axis, indicating substantial alterations in gut microbiota composition induced by LPS. Notably, the SeMet+LPS group showed an intermediate distribution between the LPS and C groups, with partial overlap toward the C group. This suggests that SeMet intervention partially restored the gut microbial structure disrupted by LPS, though complete reversion to the control state was not achieved. LEfSe analysis revealed significant differences in microbial enrichment patterns between groups (LDA score > 2.0, $P < 0.05$). The C group showed enrichment of 12 bacterial genera, while the LPS group exhibited only 2 significantly enriched genera, indicating substantial depletion of beneficial microbiota. Notably, SeMet intervention partially restored microbial diversity, with the SeMet+LPS group demonstrating enrichment of 6 genera compared to 4 in the LPS group, suggesting that SeMet effectively mitigated the LPS-induced reduction in key microbial taxa (Fig. 7C). Phylogenetic analysis revealed distinct microbial compositional patterns among experimental groups at multiple taxonomic levels (Fig. 7D). The tree illustrates the abundance distribution across different phyla and their respective classifications. Notably, Bacteroidetes (abundance of 515,783) includes Bacteroides (195,079) as the predominant species, followed by Alistipes (9,460). In the Firmicutes phylum (abundance of 199,733), key groups include Bacilli (19,417) and Lactobacillales (15,741), with Lactobacillus showing an abundance of 14,792. The Proteobacteria phylum (abundance of 52,917) is primarily represented by Gammaproteobacteria (30,677) and Deltaproteobacteria (19,399). The genus level analysis of gut microbiota showed that the C group mainly consisted of symbiotic genera, including Bacteroidetes, Rikenellaceae RC9 gut group, and Lactobacillus, with healthy microbial characteristics. LPS challenge induced significant dysbiosis, marked by reduced abundance of beneficial Faecalibacterium ($P < 0.05$) and expansion of potentially pathogenic Desulfovibrio ($P < 0.05$).

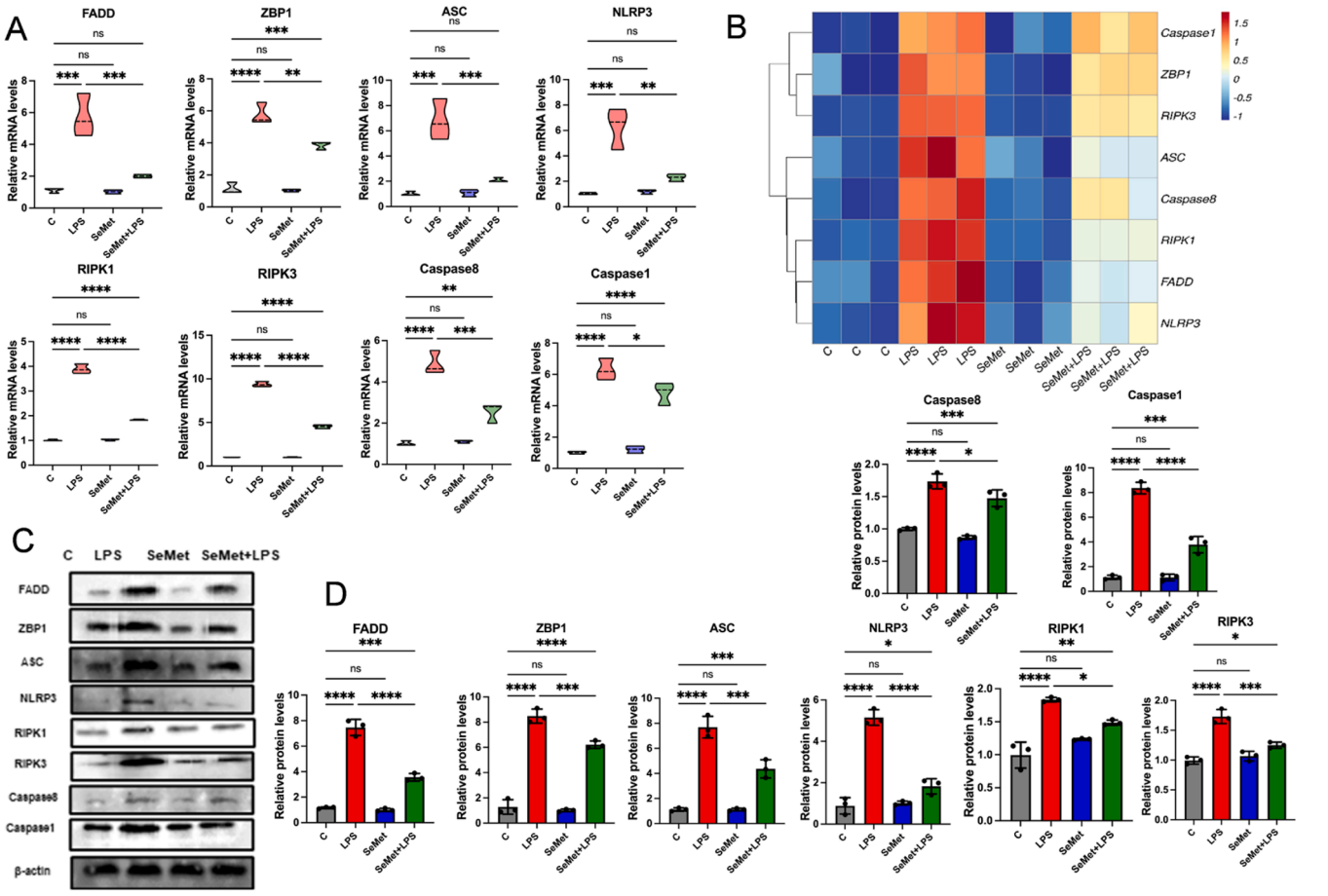

Fig. 4. Effects of SeMet and/or LPS on the assembly of PANoptosome in chicken cecal tissue. (A) qPCR results of PANoptosome-related members, $n = 3$. (B) Heatmap depicting mRNA expression changes of PANoptosome-related members, $n = 3$. (C) Western blot analysis of PANoptosome-related proteins, $n = 3$. (D) Quantitative results of protein expression changes in PANoptosome-related members, $n = 3$.

Notably, SeMet supplementation partially reversed these alterations ($P < 0.05$). These findings indicate that SeMet exerts protective effects by selectively modulating gut microbial composition, promoting beneficial taxa while suppressing LPS-induced pathogenic expansion. (Fig. 7E).

Discussion

As a biologically active organic Se compound, SeMet represents an optimal nutritional Se source for human and animal consumption. Its structural similarity to methionine enables non-selective protein incorporation, creating tissue Se stores that support endogenous selenoprotein production. SeMet supplementation has been shown to prevent or ameliorate the development of various organ-related diseases, particularly those with high metabolic and antioxidant demands (Xu et al., 2024). Research has demonstrated that SeMet effectively inhibits lipid peroxidation, promotes cell proliferation, and reduces the incidence of ferroptosis, thereby mitigating alcohol-induced hepatocyte damage (Chen et al., 2025). During mastitis, SeMet treatment alleviates *N. cyriacigeorgica* infection-induced inflammation and tissue structural damage by inhibiting ROS-mediated apoptosis (Assabayev et al., 2024). In poultry nutrition, SeMet possesses greater assimilative efficiency and prolonged bodily retention than inorganic Se, providing combined anti-inflammatory, antioxidant, and growth-promoting effects (Chen et al., 2024). Our experimental results demonstrate that SeMet suppresses LPS-triggered activation of the ROS/MAPK cascade, downregulates JNK/ERK/p38 expression, blocks PANoptosome formation and PANoptosis, while ameliorating cecal inflammatory responses, epithelial barrier dysfunction, and microbial dysbiosis.

Oxidative stress represents a fundamental pathological and physiological process ubiquitously observed in both humans and animals. The intestinal tissue, owing to its distinctive physiological milieu, exhibits heightened susceptibility to damage induced by excessive ROS (Liu et al., 2024). The Keap1/Nrf2 pathway, a pivotal cellular antioxidant defense mechanism, orchestrates the maintenance of redox homeostasis through the regulation of downstream gene expression. In physiological states, Nrf2 migrates to the nucleus and interacts with ARE regions, stimulating expression of phase II detoxification enzymes including HO-1 and NQO1 (Guo et al., 2025). Nonetheless, an overabundance of ROS can disrupt the normal functionality of this pathway, culminating in the impairment of the cellular antioxidant defense system (Chen et al., 2022). Previous studies have shown that silica treatment inhibits the Keap1/Nrf2 pathway in mouse lymphocytes, leading to decreased NQO1 and HO-1 production and ultimately compromising cellular antioxidant defenses (Li et al., 2024). Quercetin supplementation has demonstrated the capacity to reverse these effects through stimulation of the Keap1/Nrf2 antioxidant pathway (Yuan et al., 2025). Research has established that ginsenoside treatment activates the Keap1/Nrf2 axis and reinstates antioxidant defenses, consequently ameliorating rat periodontitis through coordinated control of cytokine networks and bone remodeling processes (Zhou et al., 2025). Supporting earlier findings, our results demonstrate that LPS exposure enhances Keap1 persistence, inhibiting Nrf2 signaling, lowering antioxidant enzyme (NQO1/HO-1) production, and culminating in reduced oxidative stress resistance. The oxidative imbalance was characterized by diminished activity of antioxidant systems (GPX, SOD, CAT, T-AOC, and GSH) and accumulation of oxidative markers (ROS, iNOS, H_2O_2, and MDA). SeMet

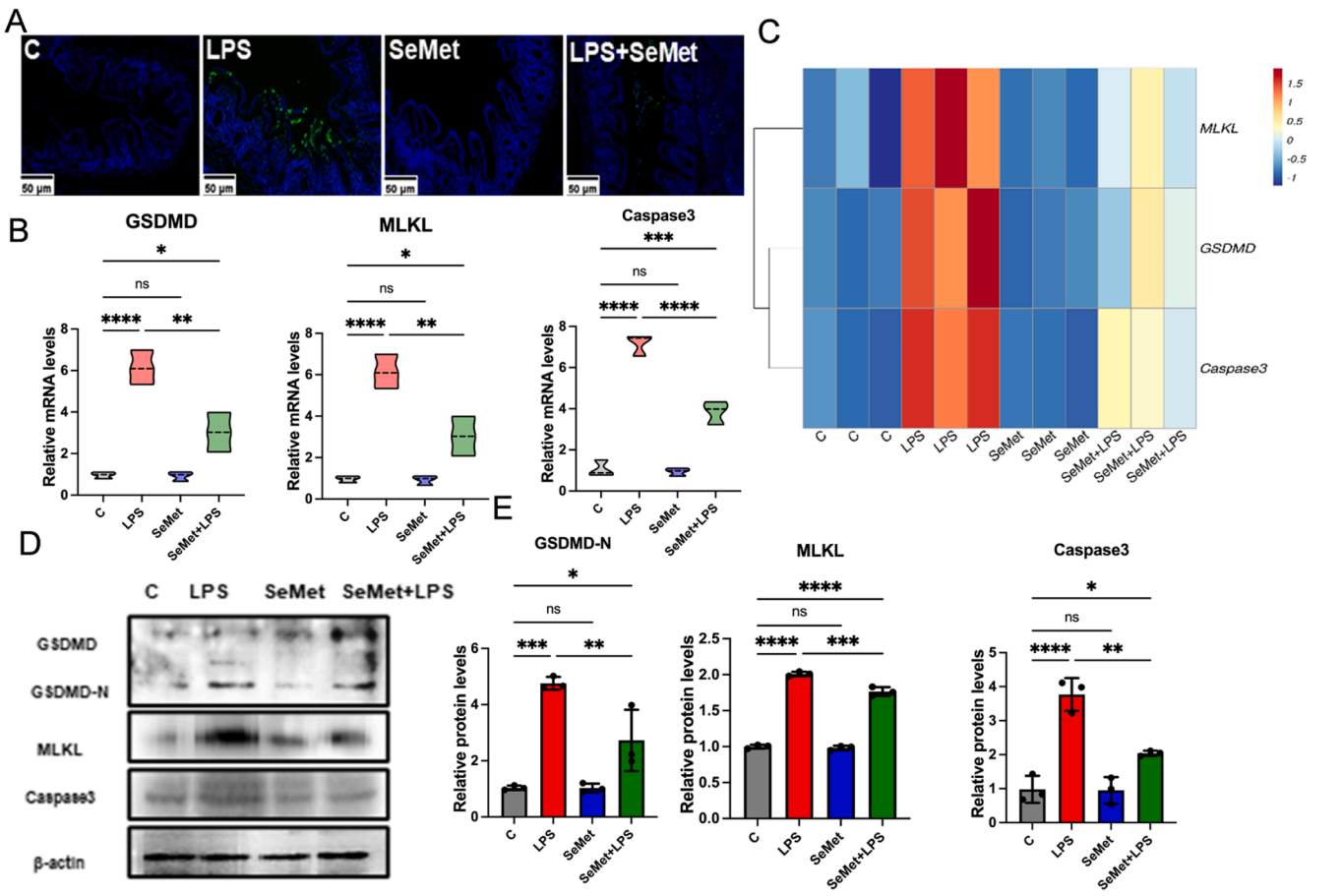

Fig. 5. Effects of SeMet and/or LPS on PANoptosis in chicken cecal tissue. (A) TUNEL staining results of chicken cecal tissue. Scale bar: 50 μm, $n = 3$. (B) qPCR results of PANoptosis-related markers, $n = 3$. (C) Heatmap illustrating mRNA expression changes of PANoptosis-related markers, $n = 3$. (D) Western blot analysis of PANoptosis-related proteins, $n = 3$. (E) Quantitative results of protein expression changes in PANoptosis-related markers, $n = 3$.

treatment reversed this imbalance through coordinated inhibition of Keap1, activation of Nrf2 signaling, and upregulation of downstream targets HO-1 and NQO1, ultimately restoring redox homeostasis.

The MAPK signaling pathway, a critical intracellular signaling system, is primarily composed of three subfamilies: p38, ERK, and JNK. Its regulatory influence spans vital cellular processes including proliferation rates, migratory capacity, apoptotic mechanisms, and inflammatory cascade activation (Huang et al., 2024). Research has demonstrated that reactive oxygen species trigger specific stimulation of the MAPK cascade, a master controller coordinating multiple regulated cell death pathways (Yu et al., 2021). In a grass carp liver cell model, exposure to DEHP was shown to activate the ROS/MAPK signaling pathway, subsequently triggering NLRP3 inflammasome activation and inducing cell pyroptosis (Cai et al., 2023). Additionally, perfluorosulfonic acid has been found to promote excessive ROS production, upregulate ERK phosphorylation levels, and induce apoptosis and necroptosis in mouse granulocytes (Fujiwara et al., 2023).

The novel programmed cell death process PANoptosis is controlled by PANoptosome activity (Zhong et al., 2025). Scientific evidence shows ZBP1 serves as an essential upstream detector that responds to distinct triggers and facilitates PANoptosome organization, mediating subsequent PANoptosis activation (Gullett et al., 2022). The initiation of MAPK cascade signaling is fundamentally linked to PANoptosome development. Contemporary studies confirm that simultaneous avermectin and microplastic exposure leads to ROS overgeneration in branchial tissues of fish, activating the MAPK pathway and promoting ZBP1-mediated PANoptosome assembly (Ju et al., 2024). Our findings further corroborate this perspective. LPS exposure activates the ROS/MAPK signaling pathway in chicken cecal tissue, promoting the assembly of ZBP1-mediated PANoptosomes and significantly upregulating the expression of PANoptosome components, including FADD, Caspase8, RIPK1, RIPK3, NLRP3, Caspase1, and ASC, thereby mediating PANoptosis in the chicken cecum. However, supplementation with SeMet ameliorates redox imbalance in chicken cecal tissue, effectively inhibiting the phosphorylation of JNK, ERK, and p38, reducing ZBP1 expression levels, and preventing PANoptosome assembly, ultimately suppressing cecal PANoptosis in chickens. These results indicate that SeMet alleviates LPS-mediated cecal PANoptosis in chickens by inhibiting the ROS/MAPK signaling pathway.

As a key pathogenic mechanism, PANoptosis actively participates in intestinal disorder initiation and progression. Experimental evidence from mouse models confirms its capacity to disturb mucosal immune regulation and drive inflammatory bowel disease formation (Gong et al., 2024). Furthermore, research has demonstrated that PANoptosis intensifies inflammatory reactions through the liberation of intracellular components and pro-inflammatory signaling molecules into surrounding tissues (Gong et al., 2022). Our results demonstrated that LPS challenge triggered PANoptotic cell death in avian cecal tissues, stimulating secretion of pro-inflammatory factors (TNF-α, COX-2, NF-κB, IL-6, IL-1β, PGE) while inhibiting anti-inflammatory IL-4. Notably, SeMet administration counteracted these effects, suppressing PANoptosis and normalizing cytokine release.

The tight junctions between intestinal cells constitute a critical natural barrier that safeguards the animal body from harmful substances by preserving the structural integrity and functionality of the intestinal epithelium (Liu et al., 2024). Tight junction proteins, including ZO-1,

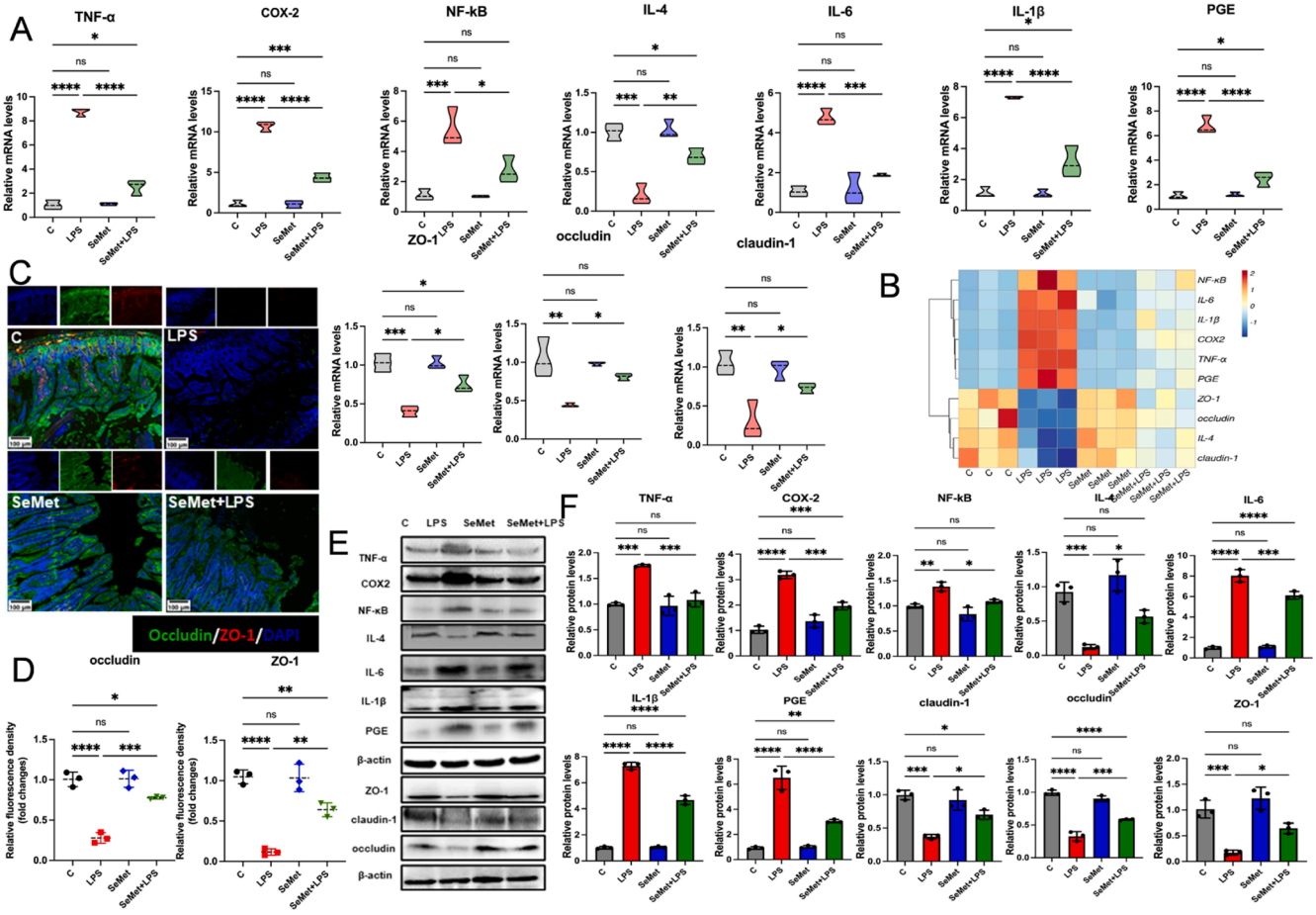

Fig. 6. Effects of SeMet and/or LPS on inflammation and tight junction proteins in chicken cecal tissue. (A) qPCR results of inflammation and tight junction-related markers, $n = 3$. (B) Heatmap depicting mRNA expression changes of inflammation and tight junction-related markers, $n = 3$. (C) Immunofluorescence staining results of occludin and ZO-1 in chicken cecal tissue. Scale bar: 100 μm, $n = 3$. (D) Quantitative analysis of occludin and ZO-1 immunofluorescence staining in chicken cecal tissue, $n = 3$. (E) Western blot analysis of inflammation and tight junction-related markers, $n = 3$. (F) Quantitative results of protein expression changes in inflammation and tight junction-related markers, $n = 3$.

claudin-1, and occludin, play essential roles in the formation and maintenance of the intestinal epithelial barrier, regulate intestinal microbiota homeostasis, and modulate osmotic balance (Bracarense et al., 2012).

Studies have demonstrated that orally delivered xylitol decreases gut-derived IL-1β and TNF-α in murine models, protects against inflammatory tight junction disruption, enhances ZO-1 protein expression, lowers Streptococcal abundance, and normalizes microbiota composition (Ma et al., 2025). Additionally, research has demonstrated that vitamin E suppresses oxidative stress and inflammatory responses, effectively reversing propoxyamine-induced impairment of tight junction proteins and rebalancing gut microbial homeostasis (Zhang et al., 2025). Morphological evaluations using H&E staining and transmission electron microscopy revealed that LPS treatment induced inflammatory factor-mediated mucosal injury, while SeMet supplementation effectively preserved intestinal barrier integrity. Protein analysis showed marked LPS-induced suppression of key tight junction components (ZO-1, claudin-1, and occludin). Fluorescence microscopy validated SeMet's efficacy in safeguarding junctional integrity by ensuring continuous production and appropriate spatial organization of these essential barrier proteins. The current findings demonstrate that SeMet exerts significant protective effects against LPS-induced gut dysbiosis through multiple microbial modulation mechanisms. The restoration of α-diversity indices and partial normalization of β-diversity patterns in the SeMet+LPS group suggest that SeMet helps maintain microbial community resilience during inflammatory challenge. Particularly noteworthy is the selective enrichment of beneficial genera like Lactobacillus, which are known to enhance gut barrier function through tight junction protein stimulation and antimicrobial peptide production. The concomitant suppression of potentially pathogenic taxa such as Desulfovibrio, which produces pro-inflammatory hydrogen sulfide, further highlights the therapeutic potential of SeMet. These microbial changes likely create a positive feedback loop, as the recovered commensals may enhance Se bioavailability through microbial redox cycling, potentially explaining the partial but significant restoration observed. These results expand our understanding of SeMet's role in gut ecosystem homeostasis beyond its classical antioxidant functions, revealing its importance as a microbial modulator.

Conclusion

In summary, this study provides compelling evidence that SeMet exerts a protective effect against LPS-induced cecal injury in chickens. Dietary supplementation with SeMet effectively mitigates oxidative stress by restoring the activity of the Keap1/Nrf2 antioxidant pathway, thereby inhibiting the activation of the ROS/MAPK signaling pathway and ultimately alleviating LPS-induced PANoptosis. This cascade of molecular events significantly enhances intestinal barrier function, reduces inflammatory responses, and effectively modulates gut microbiota dysbiosis. These findings establish an important mechanistic basis for utilizing SeMet in poultry nutrition while demonstrating its potential to improve gut health and disease resistance in commercial flocks.

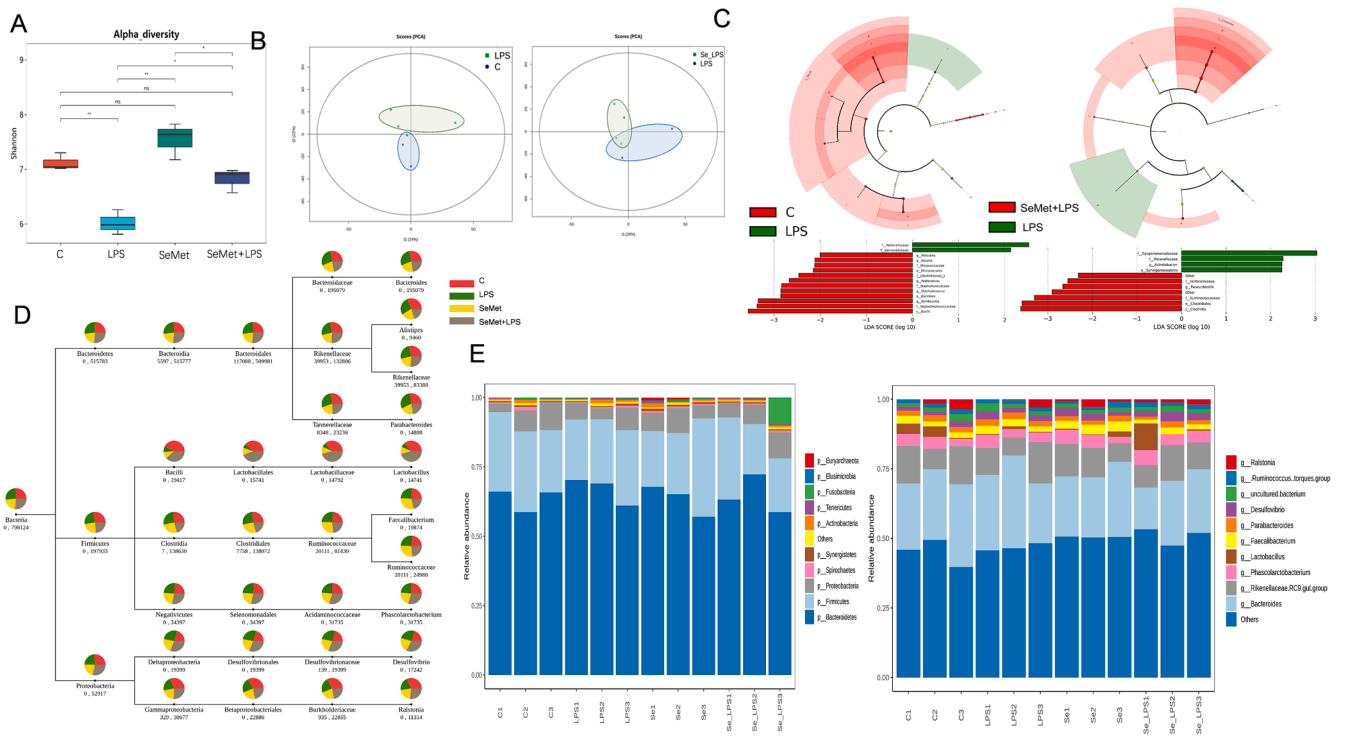

Fig. 7. Changes in gut microbiota composition. (A) α-diversity comparisons (B) β-diversity comparisons (C) LEfSe analysis identifying differentially enriched taxa (D) Phylogenetic analysis at multiple taxonomic levels (E) Relative abundance of bacterial phyla and genus.

Funding

This work was supported by the Natural Science Foundation of Heilongjiang Province of China (LH2024C025), and the Natural Science Foundation of Heilongjiang Province of China (ZD2023C002)

Data availability statement

The datasets used and/or analyzed during the current study are available from the corresponding author upon reasonable request.

CRediT authorship contribution statement

Dan Chen: Writing – original draft, Investigation. **Huanyi Liu:** Writing – original draft, Investigation. **Wenying Sun:** Software. **Shiwen Xu:** Formal analysis, Writing – review & editing.

Declaration of competing interests

The authors declare that they have no known competing financial interests or personal relationships that could have appeared to influence the work reported in this paper.

Acknowledgement

We gratefully thanks to the members of Veterinary Internal Medicine Laboratory, Key Laboratory of Experimental Animals and Embryo Biotechnology Laboratory of College of Life Sciences of Northeast Agricultural University.

Supplementary materials

Supplementary material associated with this article can be found, in the online version, at doi:10.1016/j.psj.2025.105392.

References

Assabayev, T., Han, J., Bahetijiang, H., Abdrassilova, V., Khan, M.A., Barkema, H.W., Liu, G., Kastelic, J.P., Zhou, X., Han, B., 2024. Selenomethionine mitigates effects of Nocardia cyriacigeorgica-induced inflammation, oxidative stress, and apoptosis in bovine mammary epithelial cells. Int. J. Mol. Sci. 25 (20).

Ballout, J., Akiba, Y., Kaunitz, J.D., Schwiertz, A., Mazzuoli-Weber, G., Breves, G., Diener, M., 2025. Alteration of the microbiota with Vancomycin and high-fibre diet affects short-chain fatty acid/free fatty acid receptor signalling in rat caecum. J. Nutr. Biochem., 109881

Bracarense, A.P., Lucioli, J., Grenier, B., Pacheco, G.D., Moll, W.D., Schatzmayr, G., Oswald, I.P., 2012. Chronic ingestion of deoxynivalenol and fumonisin, alone or in interaction, induces morphological and immunological changes in the intestine of piglets. Br. J. Nutr. 107 (12), 1776–1786.

Burrello, C., Garavaglia, F., Cribiù, F.M., Ercoli, G., Lopez, G., Troisi, J., Colucci, A., Guglietta, S., Carloni, S., Guglielmetti, S., Taverniti, V., Nizzoli, G., Bosari, S., Caprioli, F., Rescigno, M., Facciotti, F., 2018. Therapeutic faecal microbiota transplantation controls intestinal inflammation through IL10 secretion by immune cells. Nat. Commun. 9 (1), 5184.

Cai, H., Li, K., Yin, Y., Ni, X., Xu, S., 2023. Quercetin alleviates DEHP exposure-induced pyroptosis and cytokine expression changes in grass carp L8824 cell line by inhibiting ROS/MAPK/NF-κb pathway. Fish Shellfish Immunol. 143, 109223.

Chen, D., Sun, W., Liu, H., Wang, K., Gao, M., Guo, L., Xu, S., 2024. SeMet alleviates LPS-induced eggshell gland necroptosis mediated inflammation by regulating the Keap1/Nrf2/HO-1 pathway. Arch. Biochem. Biophys. 751, 109847.

F. Chen, Z. Zhou, J. Fu, C. Gao, Selenomethionine alleviates alcohol-induced liver injury by inhibiting ferroptosis, digestive diseases and sciences (2025).

Chen, H., Chen, J., Shi, X., Li, L., Xu, S., 2022. Naringenin protects swine testis cells from bisphenol A-induced apoptosis via Keap1/Nrf2 signaling pathway. BioFactors (Oxford, England) 48 (1), 190–203.

Chen, X., Wang, Y., Zhang, M., Du, Y., He, Y., Li, S., 2024. Selenomethionine alleviates kidney necroptosis and inflammation by restoring lipopolysaccharide-mediated mitochondrial dynamics imbalance via the TLR4/RIPK3/DRP1 signaling pathway in laying hens. Poult. Sci. 103 (12), 104439.

Chen, Y., Zhang, S., Gao, X., Hao, Z., Guo, Y., Wang, Y., Yuan, J., 2024. Selenium nanoparticles affect chicken offspring's intestinal health better than other selenium sources. Poult. Sci. 103 (12), 104367.

Fujiwara, N., Yamashita, S., Okamoto, M., Cooley, M.A., Ozaki, K., Everett, E.T., Suzuki, M., 2023. Perfluorooctanoic acid-induced cell death via the dual roles of ROS-MAPK/ERK signaling in ameloblast-lineage cells. Ecotoxicol Env. Saf 260, 115089.

Gong, W., Liu, Z., Wang, Y., Huang, W., Yang, K., Gao, Z., Guo, K., Xiao, Z., Zhao, W., 2024. Reprogramming of treg cell-derived small extracellular vesicles effectively prevents intestinal inflammation from PANoptosis by blocking mitochondrial oxidative stress. Trends Biotechnol.

Gong, W., Yang, K., Zhao, W., Zheng, J., Yu, J., Guo, K., Sun, X., 2022. Intestinal gasdermins for regulation of inflammation and tumorigenesis. Front. Immunol. 13, 1052111.
Gullett, J.M., Tweedell, R.E., Kanneganti, T.D., 2022. It's all in the PAN: crosstalk, plasticity, redundancies, switches, and interconnectedness encompassed by PANoptosis underlying the totality of. Cell Death-Assoc. Biol. Eff. Cells 11 (9).
Guo, M., Fu, W., Zhang, X., Li, T., Ma, W., Wang, H., Wang, X., Feng, S., Sun, H., Zhang, Z., Zuo, S., Wang, Z., Xu, H., 2025. Total flavonoids extracted from the leaves of Murraya paniculata (L.) Jack prevents acetaminophen-induced liver injury by activating Keap1/Nrf2 and PI3K/AKT/mTOR signaling pathway. J. Ethnopharmacol. 344, 119562.
Huang, Z., Zhong, H., Li, T., Wang, Z., Chen, X., Zou, T., You, J., Chen, J., 2024. Selenomethionine alleviates deoxynivalenol-induced oxidative injury in porcine intestinal epithelial cells independent of MAPK pathway regulation. Antioxidants (Basel, Switzerland) 13 (3).
Jia, K., Shi, P., Zhang, L., Yan, X., Xu, J., Liao, K., 2025. Trans-cinnamic acid alleviates high-fat diet-induced renal injury via JNK/ERK/P38 MAPK pathway. J. Nutr. Biochem. 135, 109769.
Ju, Z., Bi, Y., Gao, M., Yin, Y., Xu, T., Xu, S., 2024. Emamectin benzoate and nanoplastics induce PANoptosis of common carp (Cyprinus carpio) gill through MAPK pathway. Pestic Biochem Physiol 206, 106202.
Kong, D., Xu, J., Zhang, Q., Luo, D., Lv, Q., Li, S., Chen, X., Wei, L., Zhu, X., Liu, Y., Zhang, Z., 2025. Selenomethionine attenuates aflatoxin B1-induced liver injury by modulating the gut microbiota and metabolites in rabbits. J. Agric. Food Chem. 73 (5), 3080–3094.
Lan, Z., Tan, F., He, J., Liu, J., Lu, M., Hu, Z., Zhuo, Y., Liu, J., Tang, X., Jiang, Z., Lian, A., Chen, Y., Huang, Y., 2024. Curcumin-primed olfactory mucosa-derived mesenchymal stem cells mitigate cerebral ischemia/reperfusion injury-induced neuronal PANoptosis by modulating microglial polarization. Phytomedicine 129, 155635.
Lee, S., Rauch, J., Kolch, W., 2020. Targeting MAPK signaling in cancer: mechanisms of drug resistance and sensitivity. Int. J. Mol. Sci. 21 (3).
Lei, Y., Sun, W., Xu, T., Shan, J., Gao, M., Lin, H., 2024. Selenomethionine modulates the JAK2 /STAT3 / A20 pathway through oxidative stress to alleviate LPS-induced pyroptosis and inflammation in chicken hearts. Biochim. Biophys. Acta. Gen. Subj. 1868 (4), 130564.
Li, K., Yang, X., Xu, T., Shi, X., Xu, S., 2024. Quercetin protects against silicon dioxide particles-induced spleen ZBP1-mediated PANoptosis by regulating the Nrf2/Drp1/mtDNA axis. Int. Immunopharmacol. 143, 113546.
Li, N., Zhang, Z., Shen, L., Song, G., Tian, J., Liu, Q., Ni, J., 2025. Selenium metabolism and selenoproteins function in brain and encephalopathy. Sci. China. Life Sci. 68 (3), 628–656.
Li, X., Xing, M., Chen, M., Zhao, J., Fan, R., Zhao, X., Cao, C., Yang, J., Zhang, Z., Xu, S., 2017. Effects of selenium-lead interaction on the gene expression of inflammatory factors and selenoproteins in chicken neutrophils. Ecotoxicol. Environ. Saf. 139, 447–453.
Liu, H., Lin, H., Xu, T., Shi, X., Yao, Y., Khoso, P.A., Jiang, Z., Xu, S., 2023. New insights into brain injury in chickens induced by bisphenol A and selenium deficiency-mitochondrial reactive oxygen species and mitophagy-apoptosis crosstalk homeostasis. Sci. Total environ. 905, 166890.
Liu, Y., Lv, X., Yuan, H., Wang, X., Huang, J., Wang, L., 2024. Selenomethionine and allicin synergistically mitigate intestinal oxidative injury by activating the Nrf2 pathway. Toxics 12 (10).
Lu, H., Zhang, Y., Zhang, X., Wang, R., Guo, T., Wang, Q., Zhao, H., Xing, M., 2024. New insights into zinc alleviating renal toxicity of arsenic-exposed carp (Cyprinus carpio) through YAP-TFR/ROS signaling pathway. Pestic. Biochem. Physiol. 205, 106153.
Ma, P., Sun, W., Sun, C., Tan, J., Dong, X., He, J., Ali, A., Chen, M., Zhang, L., Wu, L., Wang, P., 2025. Using gut microbiota and non-targeted metabolomics techniques to study the effect of xylitol on alleviating DSS-induced inflammatory bowel disease in mice. BMC Immunol. 26 (1), 18.
Mahima, A.K.V., Kumar, A., Rahal, A., Kumar, V., Roy, D., 2012. Inorganic versus organic selenium supplementation: a review. Pak. J. Biol. Sci.: PJBS 15 (9), 418–425.
Pandeya, A., Kanneganti, T.D., 2024. Therapeutic potential of PANoptosis: innate sensors, inflammasomes, and RIPKs in PANoptosomes. Trends Mol. Med. 30 (1), 74–88.
Pecoraro, B.M., Leal, D.F., Frias-De-Diego, A., Browning, M., Odle, J., Crisci, E., 2022. The health benefits of selenium in food animals: a review. J. Anim. Sci. Biotechnol. 13 (1), 58.
Soares de Oliveira, A.R., Jayanne Clímaco Cruz, K., Beatriz Silva Morais, J., Rocha Dos Santos, L., Rodrigues de Sousa Melo, S., Fontenelle, L.C., Santos de Sousa, G., Costa Maia, C.S., Oliveira Duarte de Araújo, C., Leal Mendes, I., Simeone Henriques, G., Costa Silva, V., do Nascimento Marreiro, D., 2021. Selenium status and oxidative stress in obese: influence of adiposity. Eur. J. Clin. Investig. 51 (9), e13538.
Song, K., Wu, Y., Tan, S., 2025. Caspases in PANoptosis. Curr. Res. Transl. Med. 73 (1), 103502.
Song, Z., Jiang, M., Wang, M., Zou, J., Chen, Z., Zheng, F., Wang, Q., 2025. MAPK pathways regulated apoptosis and pyroptosis in respiratory epithelial cells of a primitive vertebrate model during bacterial infection. Int. J. Biol. Macromol. 286, 138587.
Tang, J.Y., He, Z., Liu, Y.G., Jia, G., Liu, G.M., Chen, X.L., Tian, G., Cai, J.Y., Kang, B., Zhao, H., 2021. Effect of supplementing hydroxy selenomethionine on meat quality of yellow feather broiler. Poult. sci. 100 (10), 101389.
Udawatte, D.J., Rothman, A.L., 2021. Viral suppression of RIPK1-mediated signaling. mBio 12 (4).
Wang, B., Cui, Y., Zhang, Q., Wang, S., Xu, S., 2021. Selenomethionine alleviates LPS-induced JNK/NLRP3 inflammasome-dependent necroptosis by modulating miR-15a and oxidative stress in chicken lungs. Met.: integr. Biometal sci. 13 (8).
Wang, X., Zhang, X., Sun, K., Wang, S., Gong, D., 2022. Polystyrene microplastics induce apoptosis and necroptosis in swine testis cells via ROS/MAPK/HIF1α pathway. Environ. Toxicol. 37 (10), 2483–2492.
Wang, Y., Huang, L., Cen, X., Liang, Y., Chen, K., 2025. Canonical MAPK signaling in auditory neuropathy. Biochim. Biophys. Acta (BBA) - Mol. Basis Dis. 1871 (3), 167619.
Wang, Y., Zhao, H., Guo, M., Fei, D., Zhang, L., Xing, M., 2020. Targeting the miR-122/PKM2 autophagy axis relieves arsenic stress. J. Hazard. Mater. 383, 121217.
Xia, Z., Gong, G., Huang, R., Goossens, T., Lemäle, O., Cardoso, D., Mallmann, B., Zhao, L., Wei, J., Deng, J., 2025. Butyric acid-based products, alone or in combination with hydroxy-selenomethionine, improve performance of laying hens in post-peak period by modulating their antioxidant, metabolic and immune status. Poult. Sci. 104 (4), 104840.
A. Xu, Y. Wang, D. Luo, Y. Xia, H. Xue, H. Yao, S. Li, By regulating the IP3R/GRP75/VDAC1 complex to restore mitochondrial dynamic balance, selenomethionine reduces lipopolysaccharide-induced neuronal apoptosis, 239(4) (2024) e31190.
Xu, T., Zhang, Y., Liu, H., Shi, X., Liu, Y., 2024. BPA exposure and Se deficiency caused spleen damage in chickens by nitrification stress-TNF-α. J. Environ. Manag. 367, 121994.
Yang, G., Wang, M., Qahar, M., He, J., Lai, Z., Li, S., He, D., Yan, X., Xiong, Z., Xiong, Z., Le, T.H., 2025. Post-burns persistent inflammation leads to kidney PANoptosis with caspases pathway activation. Heliyon 11 (1), e41485.
Yang, X., Li, K., Chen, X., Liu, H., Lei, Y., Xu, S., 2025. New insights into quercetin restoring the impairment of testicular angiogenesis induced by silicon dioxide particles in food: inhibiting ROS/pparγ-mediated ferroptosis. J. Agric. Food Chem. 73 (9), 5526–5536.
Yu, Y.H., Lai, Y.H., Hsiao, F.S., Cheng, Y.H., 2021. Effects of deoxynivalenol and mycotoxin adsorbent agents on mitogen-activated protein kinase signaling pathways and inflammation-associated gene expression in porcine intestinal epithelial cells. Toxins 13 (5).
Yuan, J., Li, Y., Miao, J., Zhang, X., Xiong, Y., Ma, F., Ding, J., He, S., 2025. Bamboo leaf flavonoids ameliorate cyclic heat stress-induced oxidative damage in broiler liver through activation of Keap1-Nrf2 signaling pathway. Poult. Sci. 104 (4), 104952.
Zhang, L., Gui, S., Liang, Z., Liu, A., Chen, Z., Tang, Y., Xiao, M., Chu, F., Liu, W., Jin, X., Zhu, J., Lu, X., 2019. Musca domestica Cecropin (Mdc) alleviates Salmonella typhimurium-induced colonic mucosal barrier impairment: associating with inflammatory and oxidative stress response, tight junction as well as intestinal flora. Front. Microbiol. 10, 522.
Zhang, M., Zhao, F., Guo, M., Duan, M., Xie, Y., Qiu, L., 2025. Vitamin E alleviates zebrafish intestinal damage and microbial disturbances caused by pyraclostrobin. Pestic. Biochem. Physiol. 208, 106221.
Zhang, Y., Qi, X., Chen, X., Zhang, J., Zhang, W., Lin, H., 2021. Dietary selenomethionine ameliorates lipopolysaccharide-induced renal inflammatory injury in broilers via regulating the PI3K/AKT pathway to inhibit necroptosis. Food Funct. 12 (10), 4392–4401.
Zhong, L., Guo, X., Deng, L., Wang, X., He, H., Wu, N., Tang, R., Chen, L., Chen, Y., Li, P., 2025. Dopant-regulated piezocatalysts evoke sonopiezoelectric and enzymatic PANoptosis for synergistic cancer therapy. Adv. sci. (Weinh. Baden-Wurtt. Ger.), e2500406.
Zhou, J., Obianwuna, U.E., Zhang, L., Liu, Y., Zhang, H., Qiu, K., Wang, J., Qi, G., Wu, S., 2025. Comparative effects of selenium-enriched lactobacilli and selenium-enriched yeast on performance, egg selenium enrichment, antioxidant capacity, and ileal microbiota in laying hens. J. Anim. Sci. Biotechnol. 16 (1), 27.
Zhou, R., Ying, J., Qiu, X., Yu, L., Yue, Y., Liu, Q., Shi, J., Li, X., Qu, Y., Mu, D., 2022. A new cell death program regulated by toll-like receptor 9 through p38 mitogen-activated protein kinase signaling pathway in a neonatal rat model with sepsis associated encephalopathy. Chin. Med. J. 135 (12), 1474–1485.
Zhou, Y., Zhang, Y., Wang, L., Liu, Y., Wang, Z., Guo, L., 2025. Ginsenoside Rg1 regulating inflammatory response and bone-remodeling through Keap1/Nrf2 signaling pathway in rats with periodontitis. Sci. Rep. 15 (1), 7478.